Structural Transformations of Graphene Exposed to Nitrogen Plasma: Quantum Chemical Molecular Dynamics Simulations

Journal:	*Physical Chemistry Chemical Physics*
Manuscript ID	CP-ART-10-2018-006159.R1
Article Type:	Paper
Date Submitted by the Author:	05-Feb-2019
Complete List of Authors:	Moon, Seokjin; Seoul National University, Department of Chemistry Hijikata, Yuh; Nagoya University, Institute of Transformative Bio-Molecules Irle, Stephan; Oak Ridge National Laboratory, Computational Science and Engineering Division

Journal Name

ARTICLE

Structural Transformations of Graphene Exposed to Nitrogen Plasma: Quantum Chemical Molecular Dynamics Simulations

Seokjin Moon,[a] Yuh Hijikata*[b] and Stephan Irle*[b,c]

Received 00th January 20xx,
Accepted 00th January 20xx

DOI: 10.1039/x0xx00000x

www.rsc.org/

Nitrogen-doped graphene (N-Graphene) has been intensively studied for tailoring the electronic property of the graphene, because different nitrogen configurations influence the electronic properties of N-Graphene in different ways. However, atomically precise control of the nitrogen configurations during the doping process remains a challenge in the synthesis of N-Graphene. Moreover, additional structural transformations of the graphene carbon network structure as a side-effect of plasma doping are little understood and are as of yet uncontrollable. Therefore, we theoretically investigated the nitrogen doping process of graphene for a range of nitrogen atom incident kinetic energies in nonequilibrium quantum chemical molecular dynamics (QM/MD) simulations. We observed and characterized prominent configurations of N-containing graphene. In analogy to similar, earlier studies of graphene plasma hydrogenation, we observed an Eley-Rideal associative desorption mechanism during the graphene plasma nitrogenation, producing molecular nitrogen. Especially for graphitic-N (Gr-N) and Stone-Wales-defect-N (SW-N) configurations, which are frequently observed in experimental studies, we discovered two typical chemical reaction mechanisms which were well categorized by two key processes: adsorption of primary nitrogen dopant and collision with a secondary nitrogen dopant. We discussed effects of the incident nitrogen energy on the formation mechanism, and propose a method to generate of Gr-N and SW-N configurations selectively by tuning the conditions with respect to the two key formation processes.

1. Introduction

Since the first successful isolation and characterization of graphene in 2004,[1] this atomically thin, ultimate 2D material and its chemical derivatives have inspired a myriad of investigations due to its large surface area,[2] high thermal conductivity, and high charge carrier mobility.[3] However, the absence of an electronic band gap at the Dirac point is one of the most prominent problems for the wide application of graphene in field-effect and molecular computing devices which require semiconducting electronic properties.[4] Therefore, Fermi level manipulation in graphene has been attempted by chemical doping in a wide variety of ways.[5] Nitrogen doping leading to N-doped graphene (N-Graphene) is among the most widely investigated strategies. The electronic properties depend sensitively on the precise structure of the formed nitrogen configurations in the carbon network.[6, 7] For example, single graphitic-N (Gr-N) configurations, in which one nitrogen atom substitutes a carbon atom in the hexagonal carbon network induce famously n-type semi-conductivity, while pyridinic-N (Py-N) configurations, in which one nitrogen atom is connected to only two carbon atoms forming a six-membered ring induce p-type semiconductivity.[6] The electronic properties of N-Graphene are also directly related to catalytic activities, for instance in the industrially important oxygen reduction reactions (ORR).[8] Because the roles of specific nitrogen configurations seem to be crucial,[10, 11] identification and control of nitrogen configurations are indispensable to improve the applicability of N-Graphene as a functional material for a wide range of applications.

Tremendous effort has been devoted to the control of the nitrogen dopant configuration, as the population of nitrogen configurations in N-graphene products critically depends on the synthetic method.[9] For instance, N-Graphene synthesized by the plasma-assisted chemical vapor deposition (PACVD) method with polymethylmetacrylate mainly features the Py-N configuration,[12] while the PACVD method with CH_4/NH_3 resulted in N-Graphene dominated by the Gr-N configuration.[13] The plasma-state ion/atom bombardment on graphene with an activated atomic nitrogen flux tends to produce N-Graphene dominated by Py-N, whereas a low energy nitrogen ion beam most favorably produces Gr-N.[14] These relationships have been highlighted in the past as they seem to offer control of the

[a] Department of Chemistry, Seoul National University, Seoul 151-747, Korea
[b] Institute of Transformative Bio-Molecules (WPI-ITbM) and Department of Chemistry & Graduate School of Science, Nagoya University, Furo-cho, Chikusa-ku, Nagoya, 464-8602, Japan
Email: hijikata@itbm.nagoya-u.ac.jp
ORICD: 0000-0003-4883-5085
[c] Computational Sciences & Engineering Division, Oak Ridge National Laboratory, Oak Ridge, Tennessee 37831-6493, United States
Email: irles@ornl.gov
ORICD: 0000-0003-4995-4991

† Electronic Supplementary Information (ESI) available: The simulation box model for PBC calculations. C–C, C–N, and N–N pair distribution functions. Optimized geometries for each configuration model by DFTB and DFT. Relative energies and bond distances calculated by DFTB and DFT. Scheme of Gr-N and SW-N to be counted. Discussion of complicated configurations containing more than two nitrogen atoms. Discussion of chemical composition and chemical bond networks (PDF). 14 MD trajectory movies in QuickTime format. See DOI: 10.1039/x0xx00000x

defects via a suitable choice of reactive species, plasma power and radiation time.[14-16] For the ion bombardment methods, theoretical studies have also been undertaken to shed light on the experimental findings from an atomic-scale point of view.[17-19] Classical molecular dynamics (MD) simulations demonstrated most efficient ion irradiation energy and mechanism for single-atom vacancy formation processes.[18] Another MD simulations with adaptive bond order potentials verified the most effective ion radiation angle with respect to the graphene plane.[17] However, bombardment simulation with low radiation energy has not been explored using quantum chemical potentials, and it can be anticipated that such bombardment by projectiles with a few eV would present rich chemistry resulting from reconstruction of covalent bond networks in graphene, rather than simply substitution of carbon atoms.

In this work, we investigated the plasma-assisted nitrogen atom bombardment process on graphene by combining the computationally economical density-functional tight-binding method (DFTB) with nonequilibrium molecular dynamics (MD) simulations (DFTB/MD). DFTB is an approximate density functional theory (DFT)[20] which allows to investigate bond formation/cleavage during MD simulations and faithfully describes isomerism in π–conjugated carbon nanomaterials.[21] Our DFTB/MD simulations shed light on frequently formed nitrogen configurations during plasma-assisted nitrogen doping process and reveal the formation mechanisms of quaternary nitrogen configurations, i.e. Gr-N configuration and Stone-Wales-defect-N (SW-N) configurations. The Gr-N configuration contains one nitrogen atom which substitutes one carbon atom of the graphene and it has almost the same structure as pristine graphene. The Stone-Wales defect is well known defects on graphene and can be created by rotation of one C–C bond, where in the SW-N defect one of the rotated carbon atoms is replaced by nitrogen. The role of the incident energy of nitrogen was examined in greater detail by analyzing all formation events of both configurations occurring during the nonequilibrium MD simulations. We discovered that all formation pathways are clearly categorized by two important factors, the configuration of nitrogen after first adsorption and the collision target of second nitrogen. Finally, we suggest a route to selective generation of nitrogen configurations via tuning of the dopant incident energy. The findings are expected to be of assistance to experimentally synthesize N-Graphene with specific nitrogen configurations for controlling the electronic and related physicochemical properties of N-Graphene.

2. Computational details and simulation details

2.1 Computational methods

All DFTB calculations were carried out using the self-consistent-charge version of DFTB (SCC-DFTB) as implemented in the DFTB+ program package version 1.2.2.[20] We did not employ spin polarization in our calculations, since the centers of spin are only loosely coupled, giving rise to a plethora of possible nearly degenerate spin states. Furthermore, spin-splittings are small in comparison to covalent bond formation, and we therefore do not expect significant influence of the spin state on the graphene chemistry. In the DFTB calculations, we adopted the mio-1-1 parameters for C and N.[22] All DFTB/MD simulations employed periodic boundary conditions (PBC) with a Monkhorst-Pack 5 × 5 × 1 *k*-point sampling. The velocity-Verlet algorithm was used for MD time integration, using a 0.5 fs time interval. For the system temperature we selected 300 K, controlled by a Nose-Hoover chain thermostat,[23] and the same value was assumed for the electronic temperature employed in the Fermi-Dirac distribution of orbital occupations.

In addition to DFTB calculations, we also performed geometry optimizations for selected gas-phase molecular model systems at the B3LYP/6-31G(d) level of theory. In these calculations, for open-shell systems, we employed the spin-unrestricted formalism. All DFT calculations were performed using the Gaussian 09 package.[24]

2.2. Nonequilibrium MD simulations of graphene bombardment by nitrogen atoms.

We prepared an orthorhombic unit cell containing a single, pristine graphene monolayer containing 72 carbon atoms in a plane perpendicular to the z axis at its center (ESI† Fig. S1). A vacuum layer of 100 Å separates the monolayers in mirror images of the unit cell. We optimized the geometry of this graphene monolayer supercell using the conjugate gradient method including the two unit cell vectors, which were 14.827 × 12.841 Å. This graphene monolayer was equilibrated in DFTB/MD simulations for 15 ps.

We then randomly collected 30 geometry snapshots from the DFTB/MD equilibration trajectory as initial structures for nitrogen atom bombardment simulations. Atomic incident energies were chosen to be 1, 2, and 4 eV in 30 trajectory replicas for each energy, starting at the 30 equilibration snapshot geometries mentioned before, and DFTB/MD simulations were performed for 50 ps. In each trajectory we added a total of 100 nitrogen atoms to the systems at regular intervals of 0.5 ps. The nitrogen atoms were generated 4 Å above the graphene sheet and “shot” towards the graphene sheet at a 90° angle with respect to the 2D plane. For each shot we randomly selected one carbon atom as target in the graphene supercell. To reduce the computational cost, we continuously removed floating free molecules formed during the simulations (such as dinitrogen) when they migrated away from the graphene sheet further than 4 Å. Some replicas had been severely damaged due to the consecutive attack of incoming nitrogen on the peripheral sites of graphene, others had been maintained its structure stably. This phenomena originated from the random selection of position at which nitrogen atoms were inserted. Therefore, we strived to demonstrate some trends of configuration changes with time

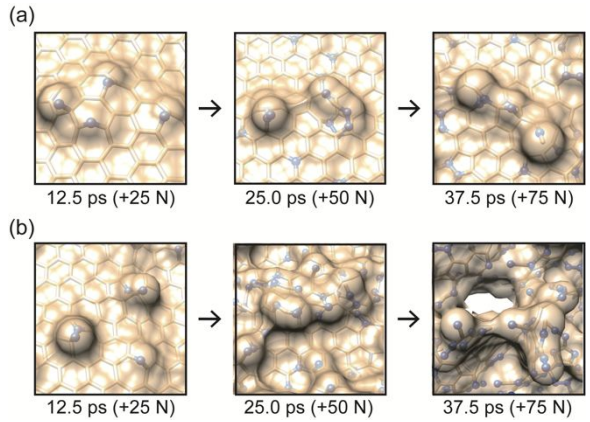

Fig. 1. Representative snapshots of the MD trajectories with the incident energy of (a) 1 and (b) 4 eV. Blue spheres and ocher sticks represent the nitrogen atoms and C–C bonds, respectively. The transparent surfaces indicate the surface of N-Graphene constructed by the van der Waals radii of nitrogen and carbon.

and nitrogen energy, and insights of nitrogen plasma doping process on graphene, rather focused on calculating any observable precisely. Similar approaches have been reported in the investigation of graphene functionalization by hydrogen and deuterium plasma, with qualitative and even quantitative agreement between simulation and experiment.[25-27] The overall process looks generally similar for representative snapshots (Fig. 1).

In addition to these 90 MD trajectories (30 trajectories × 3 different incident energies), we carried out a series of short simulations for 5 ps, in which 10 nitrogen atoms were shot, using 1, 2, 3, 4, and 5 eV as incident energies, in order to analyze the formation mechanism of Gr-N and SW-N configurations with greater possibility of observation. In these cases, we used 50 replicas with independent initial graphene geometries for each incident energy in a total 250 MD trajectories (50 trajectories × 5 different incident energies).

2.3. Analysis of trajectories.

We analyzed the connectivity relation of each atom in the obtained graphene by constructing adjacency matrices at intervals of 0.5 ps. We adopted 1.6 Å as the cut-off length to determine the number of C–C, C–N and N–N chemical bonds, because pair distribution functions for these bonds are clearly split around 1.6 Å (ESI† Fig. S2). The connectivity relations were used to specify the molecules detached from graphene, to recognize specific configurations, and to count the number of ring structures formed by chemical bonds. In addition to the trajectory analysis, we optimized some specific configurations observed in the MD trajectories at DFTB/mio-1-1 and B3LYP/6-31G(d) levels of theories. We constructed finite-size models of N-Graphene containing each specific configuration terminated by hydrogen atoms at the edge, namely $C_{66}H_{22}N_1$ and $C_{66}H_{22}N_2$ (ESI† Figs. S3, S4). In the B3LYP calculations, the spin state was assumed to be doublet and singlet, respectively. B3LYP relative energies were calculated as the difference of the total energy of each model with the sum of total energies of the pristine graphene model and an appropriate number of nitrogen molecules.

3. Results and discussions

3.1. General features of plasma doping simulations

The chemically least intrusive configuration was chemisorption of the nitrogen atom on a C–C bond, leading to an aziridinyl radical structure, which was formed under all simulated conditions. The chemisorption of nitrogen atoms elongates the neighboring C–C bonds, as the π–conjugation is necessarily interrupted, making it easier for subsequently added nitrogen atoms to react with the affected graphene carbon atoms. As a result, more nitrogen atoms are adsorbed in the vicinity of the aziridinyl radical, and structural changes in the carbon network as well as greater diversity of nitrogen configurations are observed. Addition of large numbers of nitrogen atoms tends to distort the graphene sheet, accelerating the structural disintegration of N-Graphene. After 100 nitrogen atoms were injected in the system, most of the N-Graphene sheets were severely damaged, with only a very few replicas not exhibiting structural damage (see ESI† Movies S1 and S2).

In addition to structural transformations of the graphene sheet, new molecular species in the gas phase were observed during the simulations. Nearly independent of the impact energy in the range from 1 to 4 eV, about one half of the projectile nitrogen atoms converted into nitrogen molecules, which represented by far the most dominant species leaving the graphene surface. This N_2 formation on the graphene surface follows the same Eley-Rideal associative dissociation mechanism[28] as H_2 formation in bombardment of graphene by hydrogen or deuterium atoms.[25, 26] Six typical molecular species generated in the trajectory replica are shown in Fig. 2, with their accumulated number of appearance in all 30 trajectory replicas for the three different incident energies. Besides the most prominently formed N_2, the CN, CN_2, and C_2N_2 molecules were the most frequently formed species for all incident energy cases, followed by N_3, CN_3, and C_2N_5. Higher incident energies tend to yield more molecules containing carbon, as could be expected. In total, 33.2, 33.3, and 29.8 molecules (including N_2) were formed on average in each trajectory where 100 nitrogen atoms were shot with incident energies of 1, 2, and 4 eV, respectively.

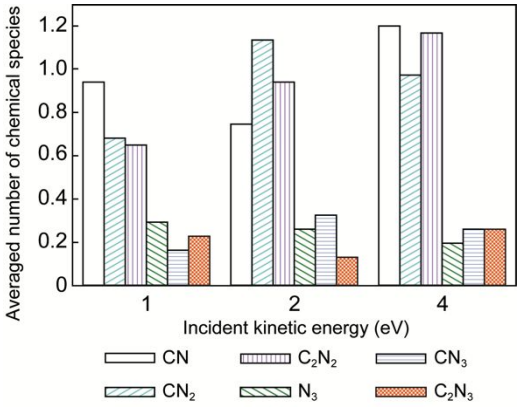

Fig. 2. The trajectory average of molecular species formation events (except N_2) during the simulations in total of 30 trajectories with the incident energies of 1, 2 and 4 eV.

A wide variety of topological changes of the graphene carbon network occurred during the simulations. We focused on identifying various configurations that may be created during the doping process in Section 3.2. We describe the formation processes and roles of simple configurations containing one or two nitrogen atoms in Section 3.2.1. For Gr-N and SW-N configurations as dominant product structures we discuss the formation mechanism of both configurations, the relationship between the formation mechanism and the incident energy, and selective generation of the configurations in Section 3.2.2. We discuss general topological changes of graphene and change of atomic composition, chemical bonds, and ring structures of carbon networks (see ESI†).

3.2. Analysis of Configurations

3.2.1 One and two nitrogen-containing configurations Two types of configuration were observed by single atomic nitrogen adsorption (SA_1 and SA_2), (Figs. 3a, b). In these figures, we use capital Roman labels to distinguish different atoms in the various adsorption sites. According to the optimized structures of SA_1 and SA_2 models (ESI† Figs. S3, S4), the corresponding C_A–C_B distances in SA_1 were ca. 0.5 Å shorter than the C_C–C_D distances in SA_2 (ESI† Table S1). In these structures, the nitrogen atom forms an aziridinyl radical triangular structure, where the dopant is either part of a three-membered ring as in SA_1, or it bridges carbon atoms as in SA_2. To elucidate the effect of the

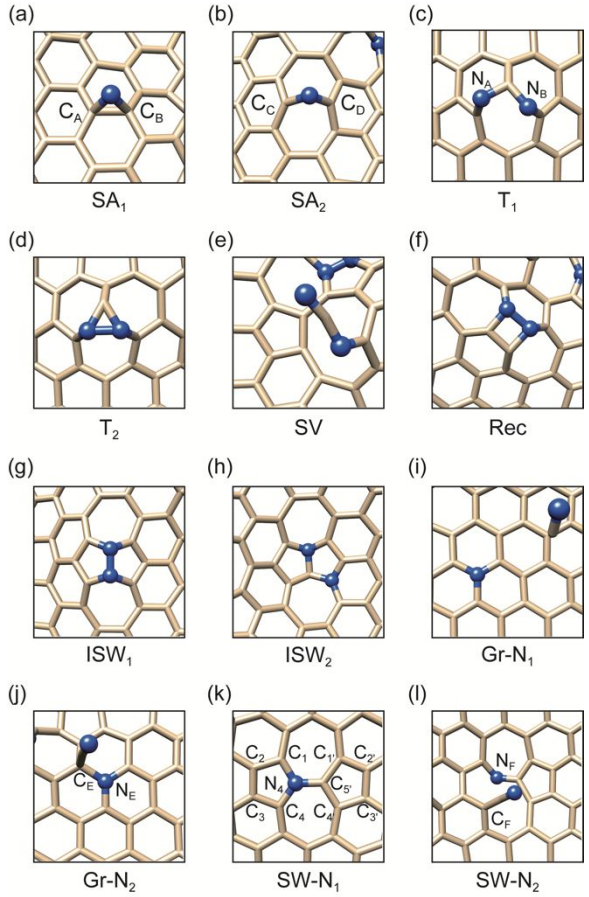

Fig 3. MD snapshots of configurations containing one or two nitrogen atoms. These configurations are (a, b) SA, (c, d) T, (e) SV, (f) Rec, (g, h) ISW, (i, j) Gr-N, and (k, l) SW-N. Blue spheres and ocher sticks represent the nitrogen atoms and C–C bonds, respectively.

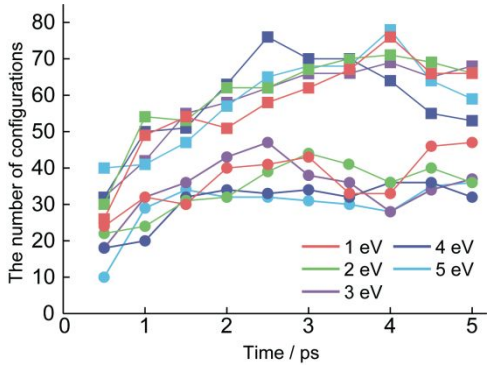

Fig. 4. The relative amount of SA_1 (circles) and SA_2 (squares) configurations counted from 50 trajectories for 5 ps (10 nitrogen atoms injection) with incident energies of 1, 2, 3, 4, and 5 eV.

incident energy of nitrogen atom on the formation of these two configurations, we counted the total number of SA_1 and SA_2 configurations from the 250 shorter MD trajectories that were run for 5 ps (10 nitrogen atoms injection) (Fig. 4).

The first bombardment of nitrogen atom on graphene can create either SA_1 or SA_2. The preference for the SA_2 configuration was gradually increased with higher incident energy, which eventually becomes sufficient to dissociate the C–C bond, required to form the SA_2 bridging structure. After the bombardment by a second nitrogen atom, the preference for the SA_2 structure was still observed, however, the dependency of the occurrence frequency on incident energy diminished. One of the prominent reasons for this moderation is the local curvature of the graphene sheet, which was theoretically studied in the case of single-walled carbon nanotubes (CNT) with different diameters[29]. Here as well it is found that SA_1 is favorable on concave surfaces while SA_2 is favorable on convex surfaces. In the case of graphene, we confirmed that both structures represent local minima on the potential surface of N-Graphene, and their energy difference at the optimized model geometry is only 0.4 eV at the DFTB level of theory.

Once the first nitrogen atom interrupts the π–conjugation of the attacked C–C bond, subsequently added nitrogen in the vicinity of the first nitrogen can create configurations containing two nitrogen atoms. When the energy of nitrogen is insufficient to detach the preexisting nitrogen atom from graphene, a new N-N bond forms and creates the triangular (T) configurations (Figs. 3c, d). Such structures were created by the migration of adsorbed nitrogen atoms to already formed SA configurations (ESI† Movie S3), or by direct nitrogen adsorption close to the SA configurations (ESI† Movie S4). Both T_1 and T_2 configurations were observed during the simulations, and both are true local minima in the DFTB method (ESI† Fig. S4). The distances between two nitrogen atoms, N_A–N_B in T_1 and N_C–N_D in T_2, were 2.170 Å and 1.459 Å respectively (Fig. 3), which indicates clear distinction between these two configurations. The two nitrogen atoms "pull up" the central carbon atom out of the graphene plane, which accelerates further structural changes including bond breaking, deformation and atomic rearrangements. For example, the Py-N configuration can be formed with a nearby third nitrogen atom, wherein the broken C–C bond of the central carbon atom is stabilized by the N-C-N moiety (ESI†

Movie S5). The T configurations can also change to the single-vacancy (SV) configurations (ESI† Fig. 3e), when a nitrogen atom in T configuration is adsorbed by an incoming nitrogen atom (the Eley-Rideal associative dissociation mechanism, see ESI† Movie S6). The direct formation of the SV configuration by bombardment with a single nitrogen was not observed in any trajectory, probably due to the high formation energy of the SV configuration.[30] When present, the SV configuration was usually accompanied by the formation of a pentagonal ring structure. This structural rearrangement is driven by the tendency of the unsaturated atoms to saturate their dangling bonds (ESI† Movie S7).[30] Clear double-vacancy configurations were rarely observed in our simulations.

We found more intrusive configurations in the graphene sheet when N-N bonds are formed, such as a rectangular (Rec) configuration (Fig. 3f) and an Inverse-Stone-Wales-defect-N (ISW) configuration (Figs. 3g, 3h). The Inverse-Stone-Wales defect in graphene consists of two pentagonal rings sharing one common side, as opposed to their separation in an ordinary Stone-Wales defect (SW) in which they are separated by a C-C bond.[31] The typical formation pathways for Rec and ISW_1 configurations, both featuring a direct N-N bond, include direct attack by an incident nitrogen atom near a pre-existing SA configuration, or by a migration of nitrogen atom along the graphene plane (ESI† Movie S8, S9). The other type of ISW (ISW_2 configuration), in which the two nitrogen atoms are separated by carbon, was also found during simulations, however, its formation process was more complex. For example, two SA_2 nitrogen atoms elongated the two C–C bonds in perpendicular direction, and a subsequent rearrangement created fused five-membered ring structures (ESI† Movie S10). The transformation of a Rec configuration in a complex atomic rearrangement can also create ISW_2 configuration (ESI† Movie S11).

Distinct from previous configurations, the Gr-N_1 and SW-N_1 configurations (Figs. 3i, 3k) are widely known as relatively stable configurations of N-Graphene, inducing a lower degree of curvature in the graphene sheet[32] because the nitrogen atom simply substitutes one carbon atom of the graphene. The formation process of these species often results in formation of CN radical species to form Gr-N_2 and SW-N_2 configurations (Figs. 3j, 3l). We noticed that the C_E–N_E distance in Gr-N_2 and the C_F–N_F distance in SW-N_2 were elongated, which means that the presence of the CN moieties weakens these bonds. The removal of the CN moiety occurred naturally during the formation processes of each configuration, or was induced by a collision with a newly injected nitrogen atom, leading to the formation of either N_2 or CN molecules. The substitutional nitrogen atom defects in graphene are prevalent desirable forms of N-Gaphene.[7, 33] Therefore, we will discuss their formation processes in greater detail in Section 3.2.2.

We calculated the relative energies of configurations containing two nitrogen atoms (Fig. 3), using model graphene systems terminated by hydrogen atoms (Fig. 5). All the configurations observed during simulations were the local minima at both of the DFTB/mio-1-1 and B3LYP/6-31G(d) level of theories, except for the T configuration. The Gr-N configurations are most stable. Although the SW-N

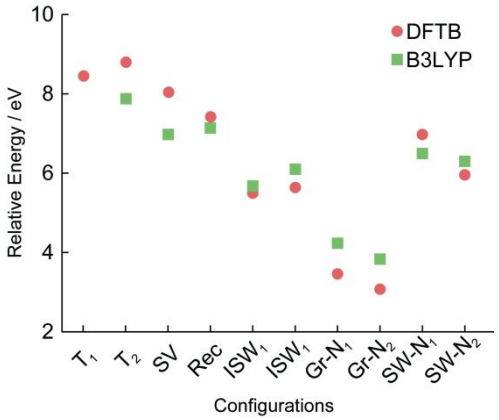

Fig. 5. Relative energies of T, SV, Rec, ISW, Gr-N, and SW-N model configurations in singlet states. The standard configuration of the relative energies was the pristine graphene ($C_{66}H_{22}$) with N_2 molecule, all have the same atomic composition. Both of the optimized T_1 and T_2 configurations in the DFT method converged to the one configuration similar to the T_2 configuration.

configurations are formed by substitution of carbon atoms like Gr-N, they have similar relative energies to ISW and Rec configurations. The T and SV configurations are less stable, which is reflected in their shorter lifetimes in our simulations.

3.2.2 The formation of Gr-N and SW-N configurations Gr-N and SW-N configurations are widely known as potentially useful configurations for valuable catalytic and electronic properties of N-Graphene,[6, 33, 34] so that it is essential to control the distribution of these configurations during synthesis.

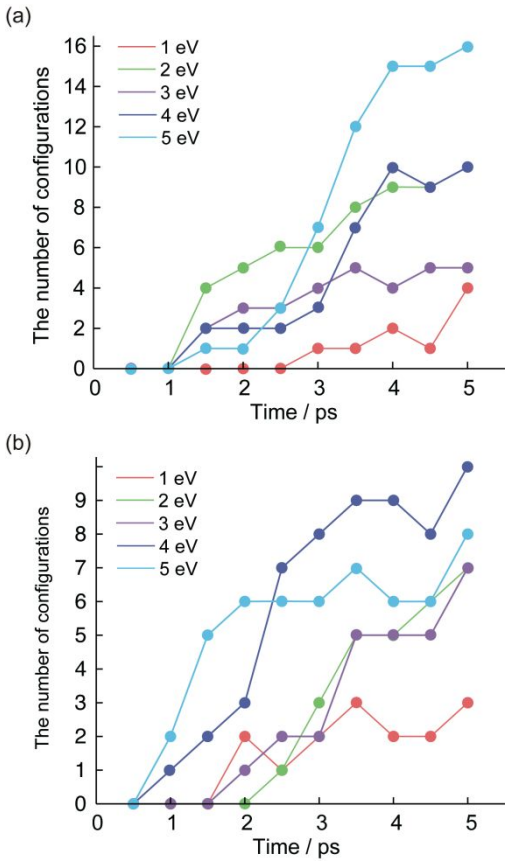

Fig. 6. The observed number of (a) Gr-N and (b) SW-N configurations counted from 50 trajectories for 5 ps (i.e. bombardment by 10 nitrogen atoms) with incident energies from 1 to 5 eV.

In this Section we discuss the possibility of controlling these formation preference via the nitrogen atom incident energy. As mentioned in Section 2.2, we prepared short 5 ps trajectories using five different projectile incident kinetic energies, namely 1, 2, 3, 4, and 5 eV with 50 replica each to allow a more quantitative analysis. We analyzed all snapshots after addition of nitrogen atom at every 0.5 ps, which amounts to 2500 snapshots from all 250 trajectories. Finally, we counted the number of Gr-N and SW-N configurations (Fig. 6) based on the criteria explained in ESI† Fig. S5.

Remarkably, even with a nitrogen atom incident energy of only 1 eV, Gr-N and SW-N configurations were observed, and an increase of the incident energies increases their number considerably. The number of observed Gr-N structures does not steadily increase with increased incident energy, as a decline is apparent at 3 eV (Fig. 6a). The number of observed SW-N, on the other, did increase continuously with increasing projectile energy. These results suggest that *the formation mechanism of these defects are not necessarily one-step processes, and their formation in multi-step processes requires less energy than reported in previous works that only considered the direct atomic substitution pathway*.[18]

In order to understand these results from a mechanistic point of view, we traced all of the formation processes of Gr-N and SW-N configurations. It was possible to categorize almost all formation pathways into two types for Gr-N and one type for SW-N, as we expected from the non-monotonous kinetic energy dependency of Gr-N (ESI† Movie S12, S13 for Gr-N, and S14 for SW-N). Schematic representations of these pathways are illustrated (Scheme 1). We named each mechanism after two important features, the initial configuration of pre-existing nitrogen and the position of targeted carbon attacked by the second incoming nitrogen. As we classified in Section 3.2.1, pre-existing nitrogen forms the SA_1 configurations with short C–C bond as well as the SA_2 configuration with a long C–C bond. In addition, we named the carbon atoms connected directly to the pre-existing nitrogen as “primary targets”, which connect to “secondary targets”. SA_1 configuration is attacked by the second incoming nitrogen at the secondary target, therefore we named this process as M_{12} (Scheme 1a). In a similar manner, the other mechanisms were named as M_{21} (Scheme 1b) and M_{22} (Scheme 1c).

We obtained three remarkable insights from the analysis (Fig. 7 and Scheme 1). First, we found that at least two nitrogen atoms were necessary to form Gr-N and SW-N configurations; pre-existing nitrogen atoms in an SA_1 or SA_2 form were indispensable to generate Gr-N and SW-N configurations. Although most of Gr-N and SW-N were created by two-step process (Scheme 1), a few processes occurred with complicated atomic rearrangements of more than two nitrogen atoms and we denoted them as “multi-step” processes. This trend was also observed in bombardment experiments with low energy nitrogen plasma where prolonged ion radiation time from 10 minutes to 20 minutes increased the amount of Gr-N configuration 3 times.[35] This result helps to understand how low energy plasma provides some valuable substitutional nitrogen configurations.

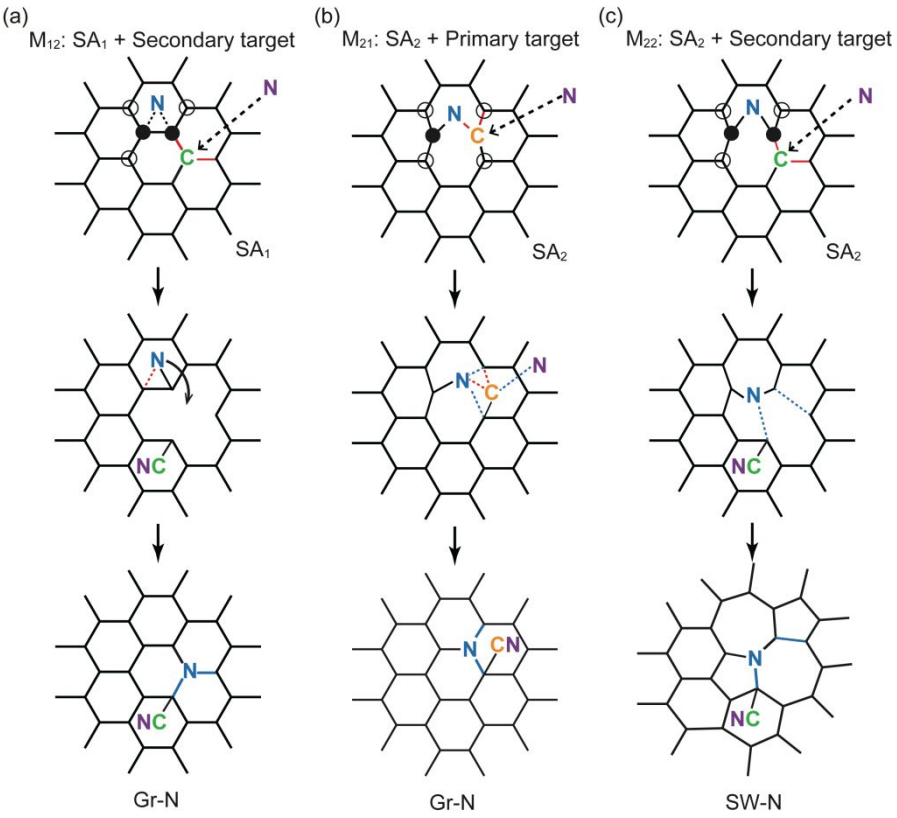

Scheme 1. The formation pathways of Gr-N and SW-N configurations. The blue and purple nitrogen indicate originally adsorbed first nitrogen and second incoming nitrogen. The red lines and blue lines indicate the chemical bonds to be broken and formed, respectively. Filled and open circles indicate primary and secondary targets, respectively.

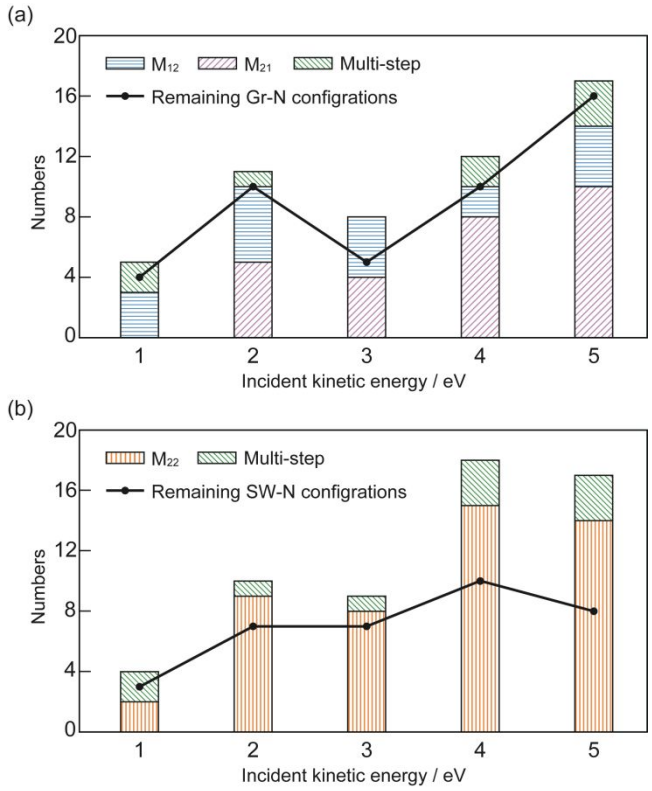

Fig. 7. The number of formation processes of (a) Gr-N and (b) SW-N by each mechanism defined (Scheme 1) depending on the incident energy of nitrogen (box graphs). The line graphs indicate the remaining configuration after simulations for 5 ps, which are the same as the numbers at 5 ps in Fig. 6.

Second, we found a preference for either Gr-N and SW-N depending on the structure of initial configurations, SA_1 or SA_2. When the processes started from the SA_1 configuration, we confirmed that SW-N was not be created at all. This might be because construction of SW-N configuration from SA_1 configuration needs to break a C–C bond between two primary carbon atoms in a six-membered ring and the first nitrogen has to insert between two primary carbon atoms. It is more favorable if two primary carbon atoms initially have long distance (M_{22}). The Gr-N configuration can be selectively generated from graphene containing SA_1 configurations. On the other hand, when the processes started from SA_2, similar amounts of GR-N and SW-N were created. They seem to be competitive with each other, which means that it is impractical to create either of them selectively. Careful attention, however, can be paid to M_{21} mechanism that does not work well with the incident energy of 1 eV to generate Gr-N configurations. As we discussed in Section 3.2.1, the energy of nitrogen atoms in the 1 eV simulations was not enough to interact with primary targets which are blocked by pre-existing nitrogen, so that the incoming nitrogen atom tends to create relatively unstable T or Rec configurations. Hence, the SW-N configuration could be selectively generated from the graphene with excess of SA_2 configurations by using low incident energy of nitrogen plasma.

Our results would be supported by experiments on CNT where the configuration formed from nitrogen adsorption can be limited to SA_2 due to the curvature of CNT. Based on the experimental bombardment studies combined with spectroscopic analysis, we confirmed that low energy plasma does not create Gr-N configurations,[36, 37] while high energy plasma do create Gr-N configurations.[38] These experimental observations are consistent with our results. Meanwhile, the detection of SW-N configuration on graphene or CNT is arduous task due to similarity of their peak positions of several spectroscopy to the prevalent “pyrrolic” nitrogen configuration so that the detection requires atomic resolution.[39]

Finally, different stabilities of SW-N and Gr-N configurations were found, according to the discrepancy between the numbers of formed and remaining configurations in each form, particularly high incident energy cases. Since larger discrepancy means lower stability, the Gr-N configurations are relatively stable to the SW-N one, which is consistent with the stability of the optimized models discussed with Fig. 5. In order to obtain N-Graphene mainly consisting of SW-N configurations, lower incident energy is more favorable. In combination with the finding that either SA_1 or SA_2 configurations can be selectively promoted by the curvature of the carbon network[29] and the reported synthetic methods of curved graphene[40] and graphene nanobubbles,[41] our finding points to a viable path to fine tune the structure of N-Graphene.

4. Conclusions

We theoretically investigated the plasma nitrogenation process of graphene based on quantum chemical molecular dynamic simulations at low incident energies between 1 to 5 eV per nitrogen atom. In particular, we focused on investigating the selective generation of specific configurations, i.e. Gr-N and SW-N configurations. As a result of first nitrogen bombardment on a pristine graphene sheet, we found two different types of “single adsorption” pattern of nitrogen dopant, where a single nitrogen atom either attaches on a C–C bond (SA_1) or inserts itself (SA_2). We observed other variations involving at least two nitrogen atoms. When secondary nitrogen atoms moderately attack regions far from the SA configurations or migrates towards them, the T, Rec, and ISW configurations (Fig. 3) are likely to be formed. Distinct from these defects, Gr-N and SW-N are substitutional configurations, which are prevalent because of inherent structural stability. They also possess valuable electronic and catalytic properties. We investigated the formation processes of these two configurations, and confirmed that there are two typical pathways to form the Gr-N configuration (M_{12} and M_{21}) and one to form the SW-N configuration (M_{22}). The key distinctions of the pathways are the pre-existing nitrogen configurations (SA_1 or SA_2), and the target carbon position to be attacked by secondary nitrogen. Since SA_1 configurations did not give rise to SW-N configuration, we conclude that Gr-N rich N-Graphene can be prepared using moderate incident energy under SA_1 rich conditions. Formation of Gr-N and SW-N from SA_2 configuration compete via M_{21} and M_{22} process, resulting in products of similar amounts of Gr-N and SW-N configurations. Nevertheless, we found that SW-N

configurations were not formed in the 1 eV incident energy case, probably because the M_{21} mechanism was interfered by steric hindrance or large barrier to approach to the primary target carbon atoms. Our findings reveal energy-resolved, atomic-level insights for the structural control of N-Graphene, and therefore its physicochemical properties.

Conflicts of interest

There are no conflicts to declare.

Acknowledgements

The authors thank to the CAMPUS Asia Support for the Formation of a Core Center (Re-inventing Japan Project Type A) by the Japan Society for the Promotion of Science (JSPS). S.I. was partially supported by the Laboratory Directed Research and Development (LDRD) Program of Oak Ridge National Laboratory. ORNL is managed by UT-Battelle, LLC, for DOE under contract DE-AC05-00OR22725. We also thank Dr. Ashi Savara at ORNL for his helpful comments on the manuscript and Professor Masamichi Yoshimura at the Toyota Technological Institute for valuable discussions.

References

1. K. S. Novoselov, A. K. Geim, S. V. Morozov, D. Jiang, Y. Zhang, S. V. Dubonos, I. V. Grigorieva and A. A. Firsov, *Science*, 2004, **306**, 666-669.
2. M. D. Stoller, S. J. Park, Y. W. Zhu, J. H. An and R. S. Ruoff, *Nano Lett*, 2008, **8**, 3498-3502.
3. A. A. Balandin, S. Ghosh, W. Z. Bao, I. Calizo, D. Teweldebrhan, F. Miao and C. N. Lau, *Nano Lett*, 2008, **8**, 902-907.
4. A. H. Castro Neto, F. Guinea, N. M. R. Peres, K. S. Novoselov and A. K. Geim, *Rev Mod Phys*, 2009, **81**, 109-162.
5. A. Lherbier, X. Blase, Y. M. Niquet, F. Triozon and S. Roche, *Phys Rev Lett*, 2008, **101**, 036808.
6. T. Schiros, D. Nordlund, L. Palova, D. Prezzi, L. Y. Zhao, K. S. Kim, U. Wurstbauer, C. Gutierrez, D. Delongchamp, C. Jaye, D. Fischer, H. Ogasawara, L. G. M. Pettersson, D. R. Reichman, P. Kim, M. S. Hybertsen and A. N. Pasupathy, *Nano Lett*, 2012, **12**, 4025-4031.
7. Z. F. Hou, X. L. Wang, T. Ikeda, K. Terakura, M. Oshima and M. Kakimoto, *Phys Rev B*, 2013, **87**, 165401.
8. G. S. Bang, G. W. Shim, G. H. Shin, D. Y. Jung, H. Park, W. G. Hong, J. Choi, J. Lee and S.-Y. Choi, *ACS Omega*, 2018, **3**, 5522-5530.
9. H. B. Wang, T. Maiyalagan and X. Wang, *Acs Catal*, 2012, **2**, 781-794.
10. H. B. Yang, J. W. Miao, S. F. Hung, J. Z. Chen, H. B. Tao, X. Z. Wang, L. P. Zhang, R. Chen, J. J. Gao, H. M. Chen, L. M. Dai and B. Liu, *Sci Adv*, 2016, **2**, e1501122.
11. D. H. Guo, R. Shibuya, C. Akiba, S. Saji, T. Kondo and J. Nakamura, *Science*, 2016, **351**, 361-365.
12. C. D. Wang, M. F. Yuen, T. W. Ng, S. K. Jha, Z. Z. Lu, S. Y. Kwok, T. L. Wong, X. Yang, C. S. Lee, S. T. Lee and W. J. Zhang, *Appl Phys Lett*, 2012, **100**, 253107.
13. D. C. Wei, Y. Q. Liu, Y. Wang, H. L. Zhang, L. P. Huang and G. Yu, *Nano Lett*, 2009, **9**, 1752-1758.
14. Y. P. Lin, Y. Ksari, J. Prakash, L. Giovanelli, J. C. Valmalette and J. M. Themlin, *Carbon*, 2014, **73**, 216-224.
15. Y. P. Lin, Y. Ksari, D. Aubel, S. Hajjar-Garreau, G. Borvon, Y. Spiegel, L. Roux, L. Simon and J. M. Themlin, *Carbon*, 2016, **100**, 337-344.
16. M. Rybin, A. Pereyaslavtsev, T. Vasilieva, V. Myasnikov, I. Sokolov, A. Pavlova, E. Obraztsova, A. Khomich, V. Ralchenko and E. Obraztsova, *Carbon*, 2016, **96**, 196-202.
17. Z. T. Bai, L. Zhang and L. Liu, *Nanoscale*, 2016, **8**, 8761-8772.
18. E. H. Åhlgren, J. Kotakoski and A. V. Krasheninnikov, *Phys Rev B*, 2011, **83**, 115424.
19. X. F. Li, K. Y. Lian, L. L. Liu, Y. C. Wu, Q. Qiu, J. Jiang, M. S. Deng and Y. Luo, *Sci Rep-Uk*, 2016, **6**, 23495.
20. B. Aradi, B. Hourahine and T. Frauenheim, *J Phys Chem A*, 2007, **111**, 5678-5684.
21. G. S. Zheng, S. Irle and K. Morokuma, *Chem. Phys. Lett.*, 2005, **412**, 210-216.
22. M. Elstner, D. Porezag, G. Jungnickel, J. Elsner, M. Haugk, T. Frauenheim, S. Suhai and G. Seifert, *Phys Rev B*, 1998, **58**, 7260-7268.
23. G. J. Martyna, M. L. Klein and M. Tuckerman, *J Chem Phys*, 1992, **97**, 2635-2643.
24. M. J. Frisch, G. W. Trucks, H. B. Schlegel, G. E. Scuseria, M. A. Robb, J. R. Cheeseman, G. Scalmani, V. Barone, B. Mennucci, G. A. Petersson, H. Nakatsuji, M. Caricato, X. Li, H. P. Hratchian, A. F. Izmaylov, J. Bloino, G. Zheng, J. L. Sonnenberg, M. Hada, M. Ehara, K. Toyota, R. Fukuda, J. Hasegawa, M. Ishida, T. Nakajima, Y. Honda, O. Kitao, H. Nakai, T. Vreven, J. A. Montgomery, Jr., J. E. Peralta, F. Ogliaro, M. Bearpark, J. J. Heyd, E. Brothers, K. N. Kudin, V. N. Staroverov, R. Kobayashi, J. Normand, K. Raghavachari, A. Rendell, J. C. Burant, S. S. Iyengar, J. Tomasi, M. Cossi, N. Rega, J. M. Millam, M. Klene, J. E. Knox, J. B. Cross, V. Bakken, C. J. Adamo, J.; Gomperts, R.; Stratmann, R. E., O. Yazyev, A. J. Austin, R. Cammi, C. Pomelli, J. W. Ochterski, R. L. Martin, K. Morokuma, V. G. Zakrzewski, G. A. Voth, P. Salvador, J. J. Dannenberg, S. Dapprich, A. D. Daniels, Ö. Farkas, J. B. Foresman, J. V. Ortiz, J. Cioslowski and D. J. Fox, *Journal*, 2009.
25. D. Haberer, C. E. Giusca, Y. Wang, H. Sachdev, A. V. Fedorov, M. Farjam, S. A. Jafari, D. V. Vyalikh, D. Usachov, X. J. Liu, U. Treske, M. Grobosch, O. Vilkov, V. K. Adamchuk, S. Irle, S. R. P. Silva, M. Knupfer, B. Buchner and A. Gruneis, *Adv Mater*, 2011, **23**, 4497-4503.
26. H. Q. Ying Wang, Zhijan Wu, and Stephan Irle, *The Journal of Physical Chemistry C*, 2017, **121**, 8480-8489.
27. A. Paris, N. Verbitskiy, A. Nefedov, Y. Wang, A. Fedorov, D. Haberer, M. Oehzelt, L. Petaccia, D. Usachov, D. Vyalikh, H. Sachdev, C. Woll, M. Knupfer, B. Buchner, L. Calliari, L. Yashina, S. Irle and A. Gruneis, *Adv Funct Mater*, 2013, **23**, 1628-1635.
28. E. Rauls and L. Hornekaer, *Astrophys J*, 2008, **679**, 531-536.
29. G. S. Zheng, Z. Wang, S. Irle and K. Morokuma, *J Am Chem Soc*, 2006, **128**, 15117-15126.
30. F. Banhart, J. Kotakoski and A. V. Krasheninnikov, *Acs Nano*, 2011, **5**, 26-41.
31. M. T. Lusk and L. D. Carr, *Phys Rev Lett*, 2008, **100**, 175503.
32. A. J. Stone and D. J. Wales, *Chem. Phys. Lett.*, 1986, **128**, 501-503.

33. G. L. Chai, Z. F. Hou, D. J. Shu, T. Ikeda and K. Terakura, *J Am Chem Soc*, 2014, **136**, 13629-13640.
34. H. Niwa, K. Horiba, Y. Harada, M. Oshima, T. Ikeda, K. Terakura, J. Ozaki and S. Miyata, *J Power Sources*, 2009, **187**, 93-97.
35. W. Zhao, O. Höfert, K. Gotterbarm, J. F. Zhu, C. Papp and H. P. Steinrück, *The Journal of Physical Chemistry C*, 2012, **116**, 5062-5066.
36. C. Morant, J. Andrey, P. Prieto, D. Mendiola, J. M. Sanz and E. Elizalde, *physica status solidi (a)*, 2006, **203**, 1069-1075.
37. C. Morant, R. Torres, I. Jimenez, J. M. Sanz and E. Elizalde, *Journal of Nanoscience and Nanotechnology*, 2009, **9**, 3633-3638.
38. F. Xu, M. Minniti, C. Giallombardo, A. Cupolillo, P. Barone, A. Oliva and L. Papagno, *Surface Science*, 2007, **601**, 2819-2822.
39. R. Arenal, K. March, C. P. Ewels, X. Rocquefelte, M. Kociak, A. Loiseau and O. Stéphan, *Nano Lett*, 2014, **14**, 5509-5516.
40. S. Zhou, J. L. Xu, Y. B. Xiao, N. Zhao and C. P. Wong, *Nano Energy*, 2015, **13**, 458-466.
41. J. Lu, A. H. C. Neto and K. P. Loh, *Nat Commun*, 2012, **3**, 823.